
Article:
Hewitt, D.A., Sundeep, S., Wang, J. et al. (2023) High frequency modelling of electric machines using finite element analysis derived data. IEEE Transactions on Industrial Electronics. ISSN: 0278-0046

https://doi.org/10.1109/tie.2023.3260357

High Frequency Modelling of Electric Machines Using Finite Element Analysis Derived Data

David A. Hewitt, Shubham Sundeep, *Student Member, IEEE,* Jiabin Wang, *Senior Member, IEEE,* Antonio Griffo *Member, IEEE*

Abstract*— The use of wide band gap semiconductor switching devices in electric machine drives leads to a significant increase in power density and efficiency compared to conventional silicon-based solutions. However, this technology also presents challenges for the insulation design of electric machines since partial discharges (PDs) may occur due to high peak voltage stress as a result of fast and high frequency switching. To evaluate the risk of PD, it is necessary to understand the voltage distribution within the windings and associated insulation of an electric machine during converter operation. To this end a suitable high frequency model of the machine windings capable of predicting the internal voltage distribution is required. This paper proposes a method of constructing such a model based on finite element analysis (FEA) derived data. The FEA data used to parameterise the model in this work incorporates frequency dependant properties and homogenisation techniques to produce data which captures the high frequency behaviour of the machine. The developed model is compared with measurements in both frequency and time domains, demonstrating the utility and accuracy of the model.

***Index Terms*— Electric machines, Equivalent circuits, Finite element analysis, Partial discharges, Wide bandgap semiconductors**

I. Introduction

Wide band gap (WBG) semiconductor devices are highly efficient and capable of switching faster than traditional silicon-based alternatives. This has made them the devices of choice in the design of new converters for use with electrical machines. The improved characteristics offered by these devices present the opportunity to achieve higher power densities and high efficiency. However, faster and higher frequency switching also lead to higher dV/dt (faster slew rates) and repetition rates which result in increased stresses being applied to the insulation systems of the electric machine. It has also been shown in literature [1] that during switching events, oscillations which occur within the machine winding and at the neutral point can result in high levels of voltage stress occurring within insulation. In the case demonstrated in literature, peak values 3.9 times larger than the dc link voltage are observed to occur in some cases.

Also due to the inductive nature of the winding, high rates of dV/dt cause an uneven distribution in voltage within the machine winding resulting in in a disproportionate amount of voltage stress being applied to the turns closest to the machine terminals during transient switching events, when compared to slower switching rates [2][3].

These increased voltages can result in voltage stresses being applied to the insulation which exceed the partial discharge inception voltage (PDIV) of the insulation material, resulting in partial discharge (PD) events occurring. These events have been shown to reduce the lifetime of the machine insulation significantly [4][5]. While it is possible to determine the level of PD activity within a machine through experimental evaluation, it is preferable to be able to assess the likely PD behaviour of a machine design prior to the production of a prototype. To achieve this is it necessary to predict, with a suitable model representing the high frequency behaviour of a machine, the voltage distributions within the machine. Data from such a model can then also be fed back into the insulation design process, allowing all insulation to be suitably specified to prevent any occurrence of PD within the organic based insulation materials of the machine.

II. High Frequency Machine Model Considerations

The construction of a high frequency electric machine model can be divided into two distinct areas of consideration: the model structure and the model parameters.

A. Model Structure

From a structural perspective machine models can be divided into two categories. The first approach [6]-[9] only attempts to model the machine on a terminal level, considering only the machine phase terminals, the neutral point, and the machine core. Models generated in this way cannot offer any insight into the voltage distribution within the machine windings making them insufficient for comprehensive PD analysis.

Manuscript received Month xx, 2xxx; revised Month xx, xxxx; accepted Month x, xxxx. This work was supported by the UKRI under Grant EP/S00081X/1. For the purpose of open access, the authors have applied a Creative Commons Attribution (CC BY) license to any Author Accepted Manuscript version arising.

D.A. Hewitt, S. Sundeep. J. Wang and A. Griffo are with the Department of Electronic and Electrical Engineering, University of Sheffield, Sheffield, S1 3JD (e-mail: David.Hewitt@Sheffield.ac.uk).

The alternative approach taken in [1]-[3][10]-[14], based on the concept of multi-conductor transmission lines (MCTL), divides the machine winding into discreet sections creating nodes at which the voltage distribution within a machine winding can be evaluated. This approach creates a more complex model which is more difficult to solve but allows the voltage distribution within the winding to be evaluated.

A further decision regarding the structure of the model is whether the model will be designed to function only at a single frequency or for a range of frequencies. A single frequency model [13][15] will have a simpler topology, but it is necessary to re-parameterise for each operating frequency/rise time; this approach can also be problematic when considering the effects of a SiC inverter in the time domain as a fixed frequency model may struggle to cope with the wide bandwidth signal generated by a SiC inverter. The alternative approach is to capture the frequency dependant behaviour of the machine using component networks, for example Foster and Cauer networks [6] or RL-ladder networks [1]-[3][12].

B. Model Parameterisation

After selecting a model topology, it is necessary to generate appropriate parameters to ensure that the model accurately represents high frequency behaviour of the machine under study. This can be done in a number of ways including by using experimental measurements [7]-[9], using analytical methods [6][10] or using finite element analysis models [1]-[3][12]-[15]. Each of these approaches has advantages and disadvantages.

Using experimental measurements can produce an impedance or S-parameter model which is well matched to the physical machine, however this approach requires a physical prototype to be manufactured, it is also only possible to characterise points on the machine which can be measured, which usually limits the model resolution to machine terminals only.

Analytical equations can potentially be used without a physical sample, however in such a case the assumptions used in the analytical equations need to accurately reflect the machine under study (for example machine geometry and type), or large mismatches between the model and physical machine will result.

FEA models present the potential to overcome the limitations of analytical equations by allowing the specific machine geometry to be considered. This approach does not come without its challenges, especially when modelling the machine at high frequency, as is necessary to achieve suitable model bandwidth for use with SiC converters. First, to reduce high frequency AC losses, multi-strand thin wires, or litz wires are often used in electric machine windings. At high frequency, the skin depth of copper wire can be of the order of a few tens of μm, and it would be impractical to mesh individual strands in a FE model. Similarly direct FE modelling of the stator and rotor lamination core requires a 3D solver with mesh sizes in the sub-skin-depth of a few μm. Such a model will take a prohibitively long time to compute with today's computational power. Furthermore, the effect of end-windings on the high frequency behaviour of machines are often ignore in high frequency modelling work reported in literature.

C. Selected Modelling Approach

This paper presents a high frequency MCTL circuit model of an electric machine based on RL-ladder networks which can predict voltage distribution on a turn-by-turn basis within an electric machine driven by a SiC inverter. The high frequency model parameters are calculated from finite element analysis (FEA) models which employ homogenisation techniques, in a manner which has not been previously applied to the parametrisation of HF electric machine models, producing improved high frequency performance within the model. This is of particular importance when considering a machine driven by a SiC based inverter due to the wide bandwidth of the resulting signals. The model is suitable for appraising the level of voltage stress which will be applied to the insulation system by a SiC inverter at the design stage so that the insulation can be suitably specified to prevent PD within the machine.

In the remainder of this paper, the methods used to perform FEA on the machine at high frequency will be introduced. After this the structure of the high frequency model employed in this work will be defined. Finally, comparisons will be performed between experimentally measured machine samples and the HF model in both the frequency and time domain.

III. FEA MODELLING

To capture high frequency behaviour of a machine in an MCTL model, its winding is discretised into a large number of segments along the direction of wave propagation. The length of a segment will be typically half or one turn in a small and medium sized machine in order to represent frequency components up to a few tens of MHz. As N number of turns in a slot are closely coupled, it is necessary to compute (N by N+1) capacitance matrices, and (N by N) inductance and resistance matrices with suitable FE models. Unless specific techniques are employed in the formulation of FEA models it is not possible to mesh the models sufficiently finely at high frequencies to obtain accurate results. In the following section the techniques which are employed in this model will be explained giving specific attention to their application to the machine under study, the specifications of which are listed in Table I.

TABLE I
MACHINE UNDER STUDY SPECIFICATIONS

Parameter	*Value*
Type	Permanent Magnet Servo Motor
Phases	3
Coils/Phase	3 in Series
Turns/Coil	66
Coil Winding	6 Parallel strands of 24.5AWG
Slot Configuration	18 slots (1 Coil/slot)
Power Rating	2.8 kW
Lamination Thickness	0.5 mm

A. Winding Homogenization

The properties of the winding in this machine are outlined in Table I. If attempts were made to model each strand of 0.4826 mm in diameter wire the model would become difficult to mesh/solve especially at higher frequencies due to the high conductor count (396 per slot). This is because as frequency increases, the skin depth of the conductors will decrease, requiring the mesh used in the model to be finer, resulting in more elements. To address this, it is necessary to employ a

homogenization technique to the winding region. Multiple methods have been proposed in literature to achieve this for stranded and litz wire including [16]-[18]. In this work, it is more suitable to utilise the homogenisation technique discussed in [16] for the machine under study as it has been employed in commercial electromagnetic tools, such as Altair-Flux, and hence is easy to use. The technique duly accounts the eddy current reaction field, and hence provides good representation of winding behaviour in high frequency range of interest. It is possible that other techniques would be better suited to other machines and should be considered in this case, such discussion is beyond the scope of this paper.

This technique requires the calculation of two equivalent parameters for the winding. Firstly, the skin effect losses of the conductor are calculated. To achieve this a single conductor cell is modelled. This cell consists of a single conductor placed within a square region; the boundaries of which have a symmetry condition applied to them. This approximates the conductor placed within an infinite array of conductors arranged with square packing. The conductor is then excited by a sinusoidal waveform of a prescribed frequency from which the resulting ac resistance (R_{ac}) is calculated. An additional simulation is performed using a dc excitation to calculate the baseline dc resistance (R_{dc})

By way of example, Fig. 1 shows the calculated R_{ac}/R_{dc} values for the conductors in this machine. Significant increase in resistance is seen when frequency is above 100kHz.

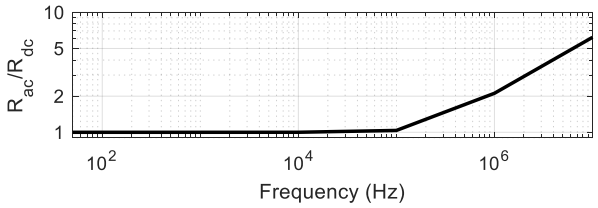

Fig. 1. Skin effect resistance contributions

The second parameter which is calculated is the frequency dependant complex permeability, which represents eddy current reaction and proximity effect. This value is calculated such that the resulting magnetic flux density within the winding region is of comparable shape and magnitude to that which would occur if the turns were modelled individually. The imaginary component of the complex permeability also represents the proximity effect losses which occur within the winding. The complex permeability of the winding region for the machine under study is shown in Fig. 2 where the winding complex permeability is expressed in the form shown in (1)

$$\mu_{complex} = \mu' - j\mu'' \quad (1)$$

where $\mu_{complex}$ is the frequency dependant complex permeability of the material, consisting of the real (μ') and imaginary components (μ'')

Considering the real component of the winding complex permeability shown in Fig. 2 it can be observed that above 100kHz the permeability of the region is reduced, this can be explained by the reduced area which the flux will penetrate into the conductors due to the impact of proximity effect, this is confirmed by considering the values presented in Fig. 1 as above this frequency the ac resistance of the strands is also observed to be increased.

The imaginary component is observed to decrease above 100kHz. It should be noted that the proximity effect losses are proportional to both the frequency and imaginary complex permeability, meaning that these losses will continue to increase above this frequency, but at a slower rate.

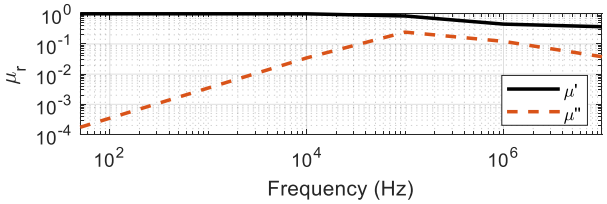

Fig. 2. Equivalent complex permeability of winding region

This approach allows the skin effect losses to be isolated from the proximity losses and modelled separately. As these losses have been shown in literature to be orthogonal [19], this is a valid approach.

To assess the efficacy of this technique an air cored inductor consisting of 100 turns was simulated, both by fully modelling the turns and using the discussed homogenisation technique. The calculated inductance of these models showed variation of 0.2% and calculated resistance showed 2% variation at 100kHz.

B. Core Complex Permeability

The core of the machine can be particularly problematic to model due to its laminated structure. To address this a frequency dependent complex permeability is employed to represent the core region [16][20][21]. This approach allows the frequency dependent anisotropic behaviour of the core to be captured without requiring the lamination stack be model on a per-lamination basis. For the machine under study, assuming the lamination properties specified in Table II, the frequency dependant complex permeability of the laminations can be calculated using equation (2) [16]. The resultant complex permeability, expressed in the form described in (1) can be observed in Fig. 3

TABLE II
CORE STEEL SPECIFICATIONS

Parameter	*Value*
Relative Permeability	1200
Conductivity	2 MS/m
Lamination Thickness	0.5mm
Stacking Factor	0.98
Tooth Width	6.5mm

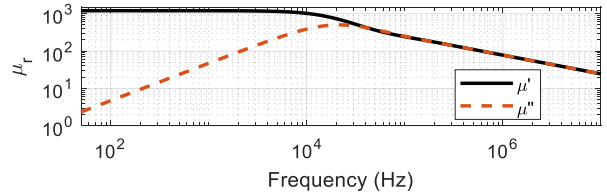

Fig. 3. Equivalent complex permeability of lamination region

$$\mu_{lam} = \frac{\mu_s \tanh((1+j)b/\delta_s)}{(1+j)b/\delta_s}, \delta_s = \sqrt{2/(\omega\sigma_s\mu_0\mu_s)} \quad (2)$$

where μ_{lam} is the frequency dependant complex permeability of the laminations, μ_s is the permeability of the lamination steel, b is half of the lamination thickness (m), ω is the angular frequency (rad/s) and σ_s is the silicon steel conductivity (S/m)

In this case the real permeability value can be observed to start decreasing at ~2kHz, at this frequency the skin depth of the steel is approximately equal to half of the lamination thickness, therefore above this frequency the effective cross-sectional area of the lamination is reduced, causing the effective permeability to also reduce. Above 30kHz the real and imaginary components have the same magnitude. This can be attributed to the fact that when the skin depth is substantially smaller than the lamination thicknesses the resulting angle of μ_{lam} converges to -45° resulting in equal magnitudes for the real and imaginary components.

C. Equivalent Core Conductivity

While the approach discussed in the previous section allows for core eddy current behaviour in the x-y plane to be captured within the FEA model, it operates on the assumption that the resultant core conductivity is zero. As a result of this, the eddy current behaviour within the lamination (z) direction of the stack is not considered. Consequently, at higher frequencies this approach can overestimate the coil inductance, as without the inclusion of eddy currents the flux will occupy the full cross-sectional area of the core material, rather than having a restricted penetration depth due to the eddy currents in the lamination direction. This difference in flux distribution will also impact the resulting calculated core losses.

To capture this behaviour, it is necessary to include an equivalent conductivity for the lamination stack. An approach for calculating the equivalent conductivity of the material is shown in (3)[22].

$$\sigma_{core} = \frac{1}{F}\left(\frac{d}{a}\right)^2 \sigma_s \tag{3}$$

where σ_{core} is the core effective conductivity (S/m), F is the lamination stacking factor, d is the lamination thickness, a is the width of the winding stack (m) and σ_s is the steel conductivity (S/m)

In this work we assume that the width of the winding stack is equal to half of the machine tooth width of symmetry. Using this, combined with the core specification listed in Table II an equivalent conductivity value for the lamination stack in the z-direction of 48,303 S/m is obtained.

D. 2D Magnetic Models

A 2D electromagnetic FEA model of the machine under study was created employing the techniques discussed in the previous sections. The geometry used in this model can be observed in Fig. 4(a). This model incorporates three machine slots (one from each phase) and employs anti-periodic symmetry to simulate the full 360° of the machine. The slot region of each winding is divided into 66 individual regions, each representing one turn of the winding. Each of these regions uses the homogenised winding properties discussed previously for its material properties. The core region of the model is represented by the frequency dependent complex permeability and equivalent conductivity for eddy current flow in the z-direction. The model was solved using an eddy current solver and was simulated using both a steel conductivity value of 0 and the equivalent conductivity value (48303 S/m) at 7 different frequencies (50, 100, 1k, 10k, 100k, 1M and 10MHz) using Ansys Electronics Desktop [23], with each simulation producing an R and L matrix for each coil, consisting of 66 rows and 66 columns. Here the diagonal elements of the matrix represent the self-inductance/resistance of each turn, and the off-diagonal elements represent the mutual inductances/resistances between the turns.

The FEA results for a single machine coil are shown in Fig. 5. As previously discussed, at high frequency the inclusion of core conductivity causes the total inductance to be reduced. This can be attributed to the fact that eddy currents induced within the core limit the depth to which flux can penetrate the core, reducing the effective cross-sectional area of the magnetic circuit, leading to a reduction in inductance. The coil resistance is also impacted. At lower frequencies, the resulting resistance increases due to the additional induced eddy currents. At higher frequencies however, the rate of increase in total resistance is observed to decrease due to the lower area of core being excited by flux, as the areas of core which are not penetrated by the flux will also not contribute to the machine losses/winding resistance.

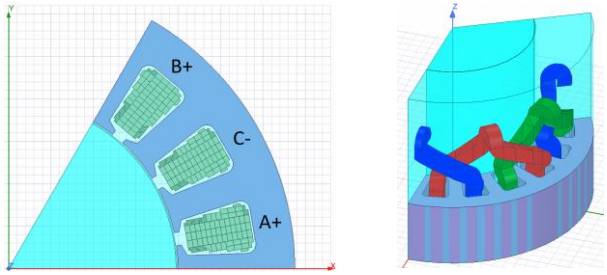

(a) (b)

Fig. 4. (a) 2D Electromagnetic FEA model of sample machine; (b) 3D Electromagnetic FEA model of sample machine

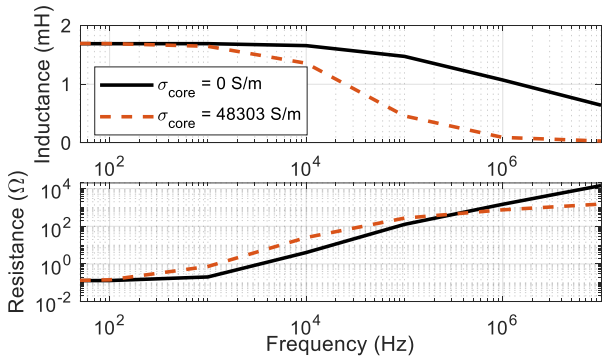

Fig. 5. 2D FEA results for single phase total coil inductance and resistance (core conductivity omitted and included)

E. End Winding Modelling

To capture the impact of the machine end winding effects a further 3D FEA model shown in Fig. 4(b) is produced. Unlike in the 2D slot model where each turn is modelled independently, in the 3D model the full coil is combined into a single entity. While this approach simplifies the model geometry, it means that the resistance and inductance values are only available on a per-coil basis, and not a turn-by-turn basis as is the case with the 2D model. Consequently, it is assumed that the end winding inductance is distributed evenly between the turns within a coil. This assumption can be justified by considering the measurements presented in [24] which show that the end winding values are relatively constant for each turn. This differs from the slot values which show much more

deviation between turns because the flux density in the end winding region is much smaller than those of the active winding in machine slots. The end winding values are extracted from the model by subtracting the total values of inductance and resistance obtained from the 2D model, on the assumption that the increase in values between the 2D and 3D model is caused by the inclusion of the end winding region. The resulting end winding inductance and resistance (per phase) is shown in Fig. 6. Considering the data presented in [24] combined with the fact that the end winding inductance is relatively small contributor to the total inductance (~25% at 1kHz) the assumption of even distribution between turns should not significantly impact the model performance.

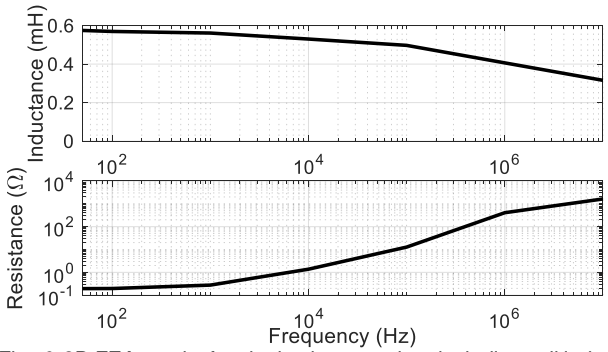

Fig. 6. 3D FEA results for single phase total end-winding coil inductance and resistance

F. Capacitance Modelling

A 2D electrostatic model of the machine slot was generated to allow the inter-turn capacitance and turn-to-ground capacitance to be calculated. This was supplemented with a 3D model of the bulk end winding region which allowed the determination of the turn-to-ground capacitance in the end winding region. In this model the winding turns are assumed to be arranged in turn order. Due to the random wound nature of this machine, this assumption cannot be guaranteed, however, the values obtained should be broadly representative of the machine, this is not an unusual assumption for random wound machines and is also made in other modelling approaches (for example [12][13][15]).

IV. High Frequency Model

A. Model Structure

The model used in this work is modular in design based on MCTL in the form of a Γ-cell topology as shown in Fig. 7 [3][12]. At the lowest level, each cell represents a single turn within a coil and is represented as a 6th order RL-ladder network (n = 6) to represent frequency dependent inductances and resistances [3][12]. As the coils in the machine under study consist of 66 turns, the model for a coil is generated by connecting 66 of the turn impedance blocks shown in Fig. 7 in series, the connections between each network being representative of start/end of each turn. The turn-to-ground capacitors are also connected between these points and the ground node. Turn-to-turn capacitances are also included in the model, however, to reduce model complexity, any capacitance below 1pF is omitted. By comparing the magnitude of the capacitance values which are included in the model this decision can be justified. Firstly, considering the turn-to-ground capacitance values, for a turn located next to the core the turn-to-ground capacitance is of the order of ~3pF – 17 pF, this is substantially larger than the values which are not located next to the core, the largest of which is 0.0024pF, which is at least 3 orders of magnitude lower than the capacitance values which are included within the model. Similarly, when the turn-to-turn capacitances are considered, the capacitance between adjacent turns is typically between ~80pF and ~120pF, whereas between non-adjacent turns the values are substantially below 1pF (typically in the fF range and below). This level of difference in capacitance is typical and demonstrated in other studies presented in literature, for example [25]. Given that the omitted capacitances are several orders of magnitude lower than the included values the omission of these capacitors will not impact the results of the model in a significant way.

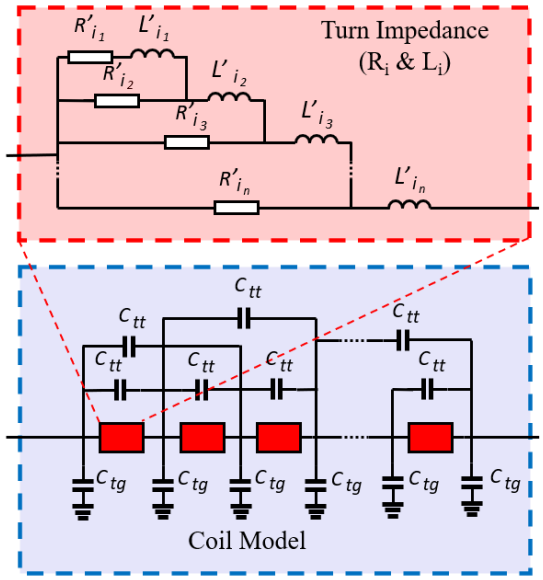

Fig. 7. MCTL model structure

A three-phase model is produced by utilizing three of the structures discussed above. The three-phase model also includes the inter-phase capacitance for the machine. Inter-phase mutual inductances are not considered in this model as the machine winding is single layer and the coupling between phases is very small relative to the coupling within phases (phase-to-phase inter-coil mutual inductance is ~7% of coil self-inductance). To create a model of the full machine three instances of the previously described block are combined in series to generate the full machine model consisting of three phases, each made up of three series connected coils.

B. Ladder Parameter Fitting

To allow the model to accurately replicate machine characteristics over a wide range of frequencies it is necessary to capture the data generated from FEA at these frequencies. Using RL-ladder networks allows the frequency dependent impedance of each turn to be represented within the model. In this model, each turn is represented by a single sixth order network and the ladder parameters ($R'i_1$ - $R'i_6$; $L'i_1$ - $L'i_6$) can

then be fitted to FE computed data including end-winding contribution using the fitting technique discussed in [3].

Briefly, this technique operates by approximating the nonlinear variation in the frequency dependant parameters as a rational function which captures the poles and residuals of the data. This is realised using the least square method of vector fitting, iteratively relocating the initial set of poles to ensure a stable pole. From these values an RL-ladder circuit which represents the rational function is calculated, further details of this process and its derivation can be found in [3]. An example of the equivalent R and L values with respect to frequency for the fitted ladder parameters of turn 1 of the coil are shown in Fig. 8 alongside the input FEA data.

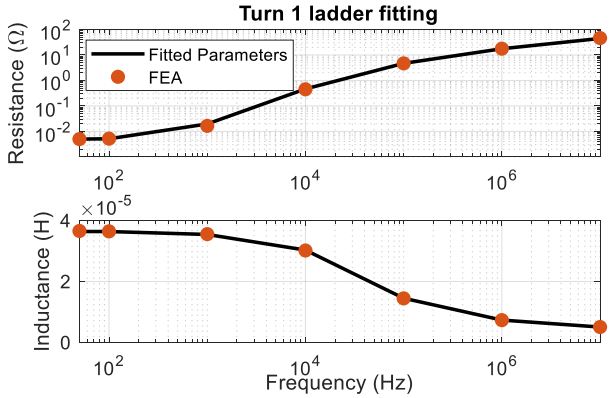

Fig. 8. Fitted ladder parameters for turn 1 of coil compared to FEA results

C. Comparison of simulated and measured common and differential mode impedances

The proposed MCTL model whose parameters are computed using the approaches described previously was simulated in the frequency domain in both three-phase differential mode and common mode configurations. For comparison the model parameterised using FEA simulations with a core conductivity of 0 S/m and the equivalent conductivity value are both evaluated. The results of these simulations, alongside the reference experimental measurements can be observed in Fig. 9 and Fig. 10.

Here Fig. 9 shows the machine in differential mode (DM) configuration and Fig. 10 shows the machine in common mode (CM) configuration. From this data several observations can be made. Firstly, both models show good agreement with the experimentally measured data at lower frequencies (below 30 kHz) however deviations are observed at higher frequencies in all cases.

Apart from a small difference in the resonant (local maximum impedance) and anti-resonant (local minimum impedance) frequencies, the predicted CM and DM impedances with the effective conductivity match broadly well with the measurement up to 1.0MHz. The differences in the resonant and anti-resonant frequencies may be attributed to the deviation of the predicted capacitances and inductances from the real values of the machine. For the capacitance predictions, the results are sensitive to the distance between conductors and core as well permittivity of insulations. Some deviations of these in the FE model from the real values of the machine are inevitable. Further, the base value of the core permeability may also differ from that of the test machine, and this will affect the accuracy of inductance predictions.

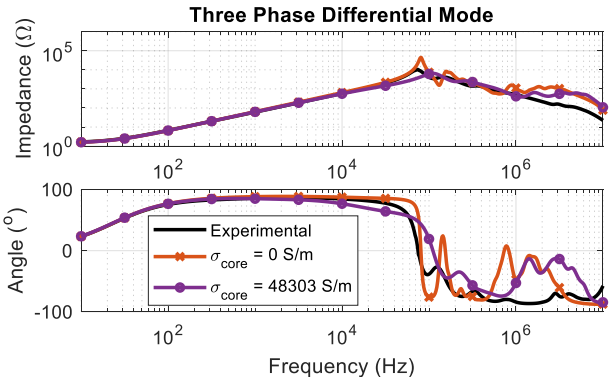

Fig. 9. Experimental and simulated frequency response of machine in three-phase differential mode configuration

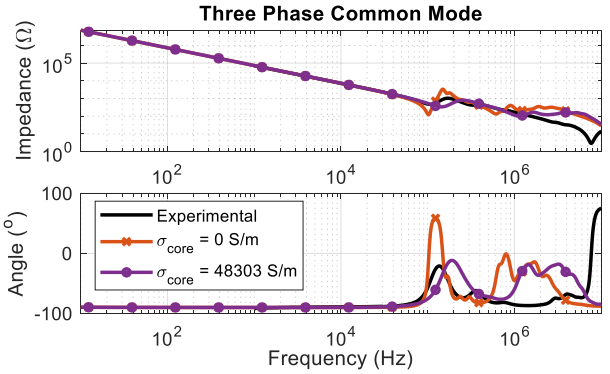

Fig. 10. Experimental and simulated frequency response of machine in three phase common mode configuration

It is also evident that the magnitude of the predicted CM and DM impedances, which result from the effective core conductivity being set to zero, differ significantly from the measurements, although the predicted resonant and anti-resonant frequencies appear to close to the measurements. These differences are mainly attributed to the mismatch in the predicted inductance and resistance when the eddy current effect in the lamination direction is neglected. Similar overshooting behaviour is also observed in the HF model presented in [25] which does not include the magnetic field effects on the core region within its model parametrisation, highlighting the importance of including this factor within the FEA modelling.

Based on these results it would be possible to further refine the FEA parameters to improve model fitting by adjusting the material properties used within the models, for example changes to the core conductivity and core permeability will impact the modelled inductance and resistance values, while change the turn order and insulation permittivity would change the capacitance values. Changes to these values would allow modelling uncertainties to be factored into the model resulting in improved fitting results. However, such a process would prevent the use of this model during the early stages of the design process, as a prototype would be required to judge any improvements in model refinement. Consequently, this approach is not discussed further here.

V. Comparison of Time Domain Simulations and Measurements

While the frequency domain performance of the model is a useful metric of how accurately the system has been characterised, from a PD analysis perspective the main metric of interest is the time domain response of the system, as this allows the voltages at various points within the machine to be studied. To this end a sample machine was connected to a 3-phase SiC inverter and excited with a 40 kHz switching frequency, and a rise time of 20ns. Waveforms at all three machine terminals and the neutral point were captured using a high bandwidth oscilloscope. Time domain simulations were then carried out using the model. To allow direct comparison with the measured results and remove the effect of the machine cables, the model machine terminals were excited using the measured terminal waveforms.

Tests were performed at modulation index values of 0.01, 0.1 and 0.5 with similar results, the results for a modulation index of 0.1 are shown in Fig. 11, where the voltages are normalised to the DC link voltage of 100V. From this simulation it can be observed that the neutral point behaviour of the machine is well captured by the model.

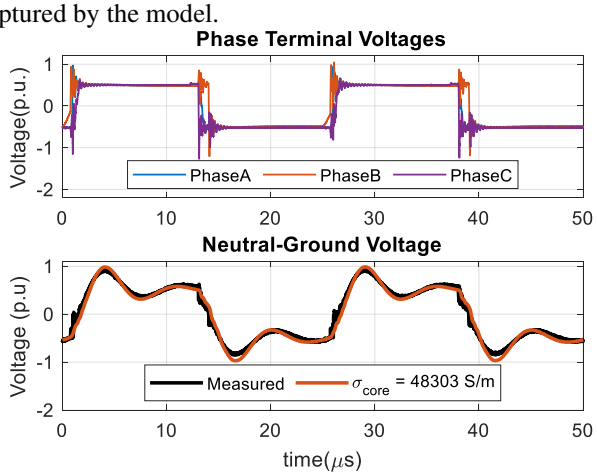

Fig. 11. Comparison of time domain simulation and experimental results of neutral point voltage

To examine the voltage distribution within the machine windings, the sample shown in Fig. 12 was manufactured which included winding taps at specific points within the first coil of the machine winding. This sample enables the predicted voltages within the machine windings be evaluated.

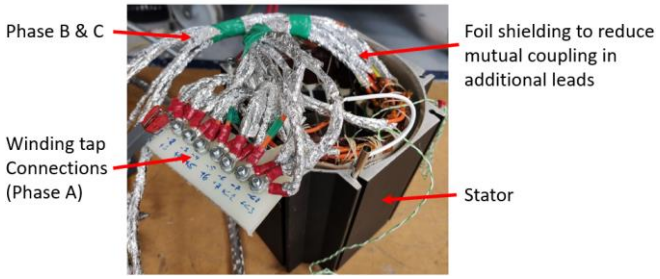

Fig. 12. Sample with tapped windings. Connection leads shielded with foil to minimise interference

Results of one such test, normalised to the DC link voltage, are shown in Fig. 13, here the converter switching frequency is 40kHz and the rise time is 20ns. From this the similarity in voltage distribution between the predictions and measurements can be observed. The process was repeated using multiple sets of measured data, the difference between the measured and simulated jump voltages are presented in Table III. From this it can be seen that the model performs comparably over multiple different sets of input data.

TABLE III
TURN 1-TURN N JUMP VOLTAGE DEVIATION FOR MULTIPLE MEASUREMENTS

Run	$\Delta Jump_{1\text{-}2}$	$\Delta Jump_{1\text{-}10}$	$\Delta Jump_{1\text{-}20}$	$\Delta Jump_{1\text{-}33}$
1	0.16 P.U.	0.35 P.U.	0.12 P.U.	0.02 P.U.
2	0.47 P.U.	0.07 P.U.	0.03 P.U.	0.03 P.U.
3	0.15 P.U.	0.32 P.U.	0.07 P.U.	0.06 P.U.
Avg	0.26 P.U.	0.25 P.U.	0.07 P.U.	0.04 P.U.

In a standard machine, the connection taps employed in this measurement would be unavailable, in such a case, the modelled results presented here would be useful for the evaluation of machine voltage distributions, for the purpose of PD evaluation. However, deviations between the predicted and measured peak voltages do exist and their causes are discussed in detail in section VI.

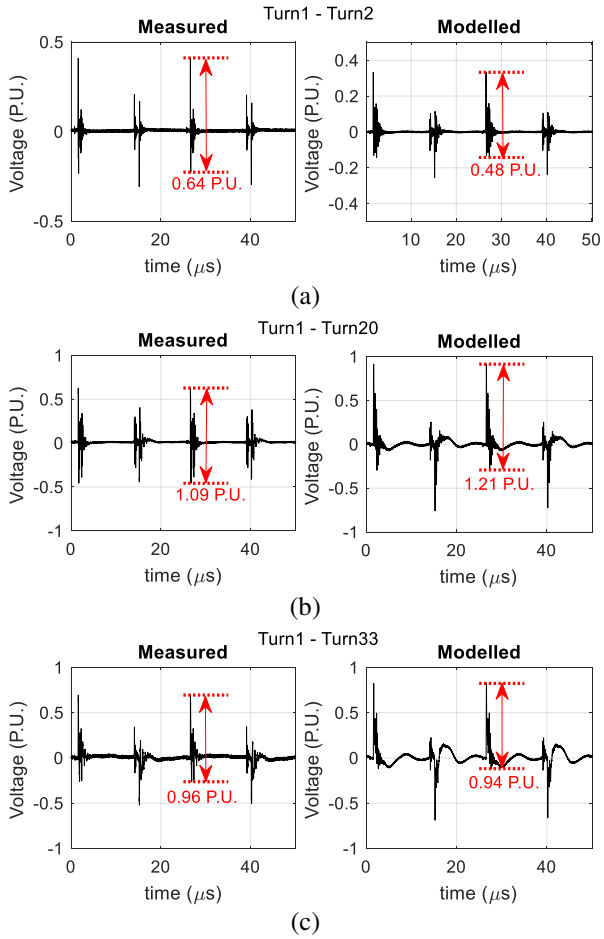

Fig. 13. Comparison of voltages within machine winding. (a) Measured between Turn 1 and Turn 2; (b) Measured between Turn 1 and Turn 20; (c) Measured between Turn 1 and Turn 33

VI. Discussion

The results presented in previous sections introduce several interesting points worthy of discussion.

A. Representation of Core Material

The use of a frequency dependent complex permeability core material to represent the core region, combined with an effective conductivity property have shown to produce FEA results which represent the measured properties of the sample machine well. These techniques allow the eddy current and loss behaviour of the core material to be captured within the FEA simulation directly. This technique also allows the impact of core eddy currents to be captured within the simulation, (for example the increased drop-off in high frequency inductance owing to reduce core flux penetration caused by the eddy currents). If these effects were to be accounted for by conventional means it would be necessary to fully capture the lamination structure within the model geometry in 3D, resulting in substantial complexity, due to the very small skin depth at high frequency.

B. Input Parameter Sensitivity

Simulations were performed for the proposed model topology using parameters derived from nominal values of σ_{core} calculated using the equations proposed in [22]. The resulting predictions showed a reasonable correlation with the measured system impedance plots in both differential and common mode configurations. From simulations it can be observed that neglecting core conductivity causes a significant deviation of the impedance magnitudes although the predicted resonant frequency and anti-resonant frequency move closer to the measured result.

As the core conductivity value is derived from an analytical equation there are a number of reasons for which this parameter may contain errors. Firstly, the equation assumes an ideal lamination stack which is perfectly insulated between the layers, in practice it is reasonable to expect that this level of perfection will not be realised. Furthermore, the analytical equation considers a simplified geometry for the core shape. While this is a reasonable approximation, it will not fully capture the behaviour of the more complicated core shape. Consequently, it is reasonable to assume that the equivalent core conductivity value may contain some degree of uncertainty.

The value of core relative permeability will also impact the model performance. The results presented here use a permeability value which represents the lamination steel being operated at a flux density of ~1.4T, while this is reasonable for the operating conditions which the machine under study was being operated, under higher load conditions the flux level would be higher, this would result in the relative permeability of the steel being reduced, particularly in areas which are operating close to saturation. To consider the impact of this the model was also tested using a relative permeability value of 600, to allow the model sensitivity to this parameter to be assessed. In this analysis it was found that this change resulted in a 6% increase in machine resonant frequency and a 3% decrease in the resonant impedance when connected in a differential configuration. The low model sensitivity to the relative core permeability can be understood by the fact that the high frequency inductance and resistance are dependent on leakage flux in the slot region which presents a dominant invariant reluctance to the leakage flux path.

While it is potentially possible to experimentally refine the material parameters value further, such refinement would require the production of prototypes so is undesirable. Considering the time domain simulations discussed in the next section, it can be concluded that refining the parameters to further improve resonant/anti-resonant frequency matching would not significantly impact the voltage predictions in this model.

C. Time Domain Model Response

Time domain simulations of the machine model were compared to experimental measurements based on sample machines. The purpose of this model is to evaluate the voltages within the machine windings for the purpose of assessing the likelihood of partial discharge activity. To achieve this a machine designer would evaluate the model predicted voltage levels and jump voltages with respect to the expected PDIV values of the machine insulation system. This comparison would allow an informed judgement to be made regarding the likelihood of PD activity within various elements of the machine insulation system.

Firstly, considering the neutral-to-ground voltage, good agreement can be observed between the peak voltage levels of the simulated and measured cases. In the case of the simulated data, it can be observed that the primary oscillation occurs at a slightly higher frequency than is the case in the measured data. This can be attributed to the previously observed frequency domain discrepancy in modelled anti-resonant frequency. From this it can be determined that although this discrepancy does impact the time domain model performance, it does not do so in a manner which significantly impedes the model performance for the purpose of PD analysis within the machine.

Secondly, considering the voltages within the machine windings, small discrepancies in peak voltage can be observed in some of the measured cases. These discrepancies can be explained by a combination of factors. Firstly, to measure the voltages within the machine winding, it was necessary to manufacture a non-standard sample which included taps within the winding. The inclusion of these winding taps slightly modifies the geometry of the winding; furthermore, the leads which allow connection to these taps will introduce additional length to the tapped turns, and additional parasitic capacitance and mutual inductance between the turns which would not otherwise be present within the machine. While these values will not significantly impact the performance of the machine, it is likely that their associated parasitic values will influence the high frequency behaviour slightly. This observation is supported by the fact that the largest discrepancy between measured and modelled results occurs in the measurements between turn 1 and turn 2. In this case, the measurement is taken across a single turn of the winding, meaning that any additional parasitic values will influence the results most heavily here. This observation is further supported by the fact that measurements across many turns (e.g., turn 1 to turn 20; turn 1 to turn 33, and the phase voltages) show a lower degree of error between the measured and modelled values.

An additional factor which will impact the machine high frequency behaviour is the arrangement of the winding turns within the machine slot. As this machine is a random wound machine, the turn distribution cannot be guaranteed. Analysis

has been performed to consider the impact of the unknown turn position on model performance, however this analysis is beyond the scope of this paper. In this analysis it was found that the arrangement of turns within the slot will have small impacts on the winding voltage distribution, especially at high frequency.

Furthermore, it is well known that the differential probes (ADP305 – 100MHz Bandwidth) used in the measurement introduce a common mode coupling and hence effect measurement accuracy at high frequency [27]. Ideally such measurements should be performed using optically coupled differential probes. Despite these factors, the model predicted peak voltages are a good representation of the measured values for the machine, making them useful for the prediction of PD behaviour. It is worth noting that in a typical machine these points would not be accessible for measurement, meaning that a model-based approach is the only option for assessment in such cases.

D. Practical use case for model

As the parameters of this model are generated using FEA data it is possible to predict the level of voltage stress which will occur within the machine insulation during the design stage without prototype production being necessary. It is also possible using data published in literature to determine the expected PDIV values of the proposed insulation system, considering the construction techniques (for example the inclusion of encapsulation materials [28]) and materials used.

One example of a use case where this would be of value can be seen by considering the sample testing outlined in [5]. Here motor samples were tested using a SiC inverter under a range of conditions to assess the impact of SiC inverters have on sample lifetime. In some of the test cases which produced PD activity the machine was operated using DC link voltages at which the machine had previously driven by a conventional Si based IGBT inverter without the occurrence of PD. In this study it was found that the primary location in which PD occurred was within the machine end windings, this can be attributed to the fact that the machine design does not incorporate a dedicated phase separator material and consequently phase-to-phase isolation is achieved using the turn level insulation only. In this case, the application of the proposed HF model would have identified that the phase-to-phase voltages would exceed the PDIV of the insulation system, necessitating a redesign of the phase-to-phase insulation system to allow this design to be operated reliably using SiC inverters.

VII. Conclusions

This paper has demonstrated a modelling approach and a machine model suitable for evaluation at high frequency. The proposed model is parameterised entirely using FEA derived data, making it suitable for use during the prototyping stage of machine design, prior to the production of prototypes.

The model is constructed on a turn-by-turn basis, making it possible to not only simulate the voltages at the machine terminals and star-neutral, but also the voltages within the machine winding, providing a useful insight into the machine voltages which would not usually be measurable.

One example use case for which this model would be particularly valuable is during the design process of electric machines for use with wide bandgap semiconductor converters, for example SiC based converters.

These converters generally apply rapidly changing, high dV/dt voltages to the machine terminals, resulting in the potential for significant voltage overshoot at the terminals and uneven voltage distributions within the machine winding. The resulting high voltages within the machine windings can result in partial discharge events occurring within the insulation systems if the insulation PDIV is exceeded.

Using the proposed model to evaluate the voltage distribution within the machine it is possible to assess the suitability and requirements of machine insulation systems during the design stage, ensuring that all insulation is suitably specified to prevent PD activity which would lead to premature machine failure. To this end, the proposed model is well suited, as it can predict not only the voltages which occur at the machine terminals, but also the voltages within the winding.

References

[1] S. Sundeep, J. Wang, A. Griffo and F. Alvarez-Gonzalez, "Antiresonance Phenomenon and Peak Voltage Stress Within PWM Inverter Fed Stator Winding," *IEEE Transactions on Industrial Electronics,* vol. 68, no. 12, pp. 11826-11836, 2021.

[2] S. Sundeep, J. Wang and A. Griffo, "Prediction of Transient Voltage Distribution in Inverter-fed Stator Winding, Considering Mutual Couplings in Time Domain," in *IEEE Energy Conversion Congress and Exposition (ECCE)*, Detroit, MI, USA , 2020.

[3] S. Sundeep, J. Wang and A. Griffo, "Holistic Modeling of High-Frequency Behavior of Inverter-Fed Machine Winding, Considering Mutual Couplings in Time Domain," *IEEE Transactions on Industry Applications,* vol. 57, no. 6, pp. 6044-6057, 2021.

[4] E. Sili, J. P. Cambronne, N. Naudé and R. Khazaka, "Polyimide lifetime under partial discharge aging: effects of temperature, pressure and humidity," *IEEE Trans. Dielectr. Electr. Insul,* vol. 20, pp. 435-442, 2013.

[5] D. Hewitt, S. Sundeep, J. Wang, A. Griffo, M. Diab and X. Yuan, "An Experimental Assessment of the Impact of High dv/dt SiC Converters on Insulation Lifetime of Electrical Machines," in *IEEE Energy Conversion Congress and Exposition (ECCE)*, Detroit, Mi, USA, 2022.

[6] J. L. Guardado, J. A. Flores, V. Venegas, J. L. Naredo and F. A. Uribe, "A machine winding model for switching transient studies using network synthesis," *IEEE Transactions on Energy Conversion,* vol. 20, no. 2, pp. 322-328, 2005.

[7] A. Boglietti, A. Cavagnino and M. Lazzari, "Experimental High-Frequency Parameter Identification of AC Electrical Motors," *IEEE Transactions on Industry Applications,* vol. 43, no. 1, pp. 23-29, 2007.

[8] B. Mirafzal, G. L. Skibinski, R. M. Tallam, D. W. Schlegel and R. A. Lukaszewski, "Universal Induction Motor Model With Low-to-High Frequency-Response Characteristics," *IEEE Transactions on Industry Applications,* vol. 43, no. 5, p. 12331246, 2007.

[9] J. Sun and L. Xing, "Parameterization of Three-Phase Electric Machine Models for EMI Simulation," *IEEE Transactions on Power Electronics,* vol. 29, no. 1, pp. 36-41, 2014.

[10] J. L. Guardado and K. J. Cornick, "A computer model for calculating steep-fronted surge distribution in machine windings," *IEEE Transactions on Energy Conversion,* vol. 4, no. 1, pp. 95-101, 1989.

[11] P. McLaren and H. Oraee, "Multiconductor transmission-line model for the line-end coil of large AC machines," *IEE Proceedings B (Electric Power Applications) ,* vol. 132, no. 3, 1985.

[12] O. Magdun, S. Blatt and A. Binder, "Calculation of stator winding parameters to predict the voltage distributions in inverter fed AC machines," in *th IEEE International Symposium on Diagnostics for*

Electric Machines, Power Electronics and Drives (SDEMPED), Valencia, Spain , 2013.

[13] M. Pastura and E. a. , "Partial Discharges in Electrical Machines for the More Electric Aircraft—Part I: A Comprehensive Modeling Tool for the Characterization of Electric Drives Based on Fast Switching Semiconductors," *IEEE Access,* vol. 9, pp. 27109-27121, 2021.

[14] Y. Xie, J. Zhang, F. Leonardi, A. R. Munoz, M. W. Degner and F. Liang, "Modeling and Verification of Electrical Stress in Inverter-Driven Electric Machine Windings," *IEEE Transactions on Industry Applications,* vol. 55, no. 6, pp. 5818-5829, 2019.

[15] G. Suresh, H. A. Toliyat, D. A. Rendusara and P. N. Enjeti, "Predicting the transient effects of PWM voltage waveform on the stator windings of random wound induction motors," *IEEE Transactions on Power Electronics,* vol. 14, no. 1, pp. 23-30, 1999.

[16] A. D. Podoltsev, K. G. N. B. Abeywickrama, Y. V. Serdyuk and S. M. Gubanski, "Multiscale Computations of Parameters of Power Transformer Windings at High Frequencies. Part I: Small-Scale Level," *IEEE Transactions on Magnetics,* vol. 43, no. 11, pp. 3991 - 3998, 2007.

[17] S. Hiruma, Y. Otomo and H. Igarashi, "Eddy Current Analysis of Litz Wire Using Homogenization-Based FEM in Conjunction With Integral Equation," *IEEE Transactions on Magnetics,* vol. 54, no. 3, pp. 1-4, 2018.

[18] S. Ehrlich, H. Rossmanith, M. Sauer, C. Joffe and M. März, "Fast Numerical Power Loss Calculation for High-Frequency Litz Wires," *IEEE Transactions on Power Electronics,* vol. 36, no. 2, pp. 2018-2032, 2021.

[19] J. A. Ferreira, "Improved analytical modeling of conductive losses in magnetic components," *IEEE Transactions on Power Electronics,* vol. 9, no. 1, pp. 127-131, 1994.

[20] K. G. N. B. Abeywickrama, A. D. Podoltsev, Y. V. Serdyuk and S. M. Gubanski, "Computation of Parameters of Power Transformer Windings for Use in Frequency Response Analysis," *IEEE Transactions on Magnetics,* vol. 43, no. 5, pp. 1983-1990, 2007.

[21] A. D. Podoltsev, K. G. N. B. Abeywickrama, Y. V. Serdyuk and S. M. Gubanski, "Multiscale Computations of Parameters of Power Transformer Windings at High Frequencies. Part II: Large-Scale Level," *IEEE Transactions on Magnetics,* vol. 43, no. 12, pp. 4076-4082, 2007.

[22] J. Wang, H. Lin, Y. Huang and X. Sun, "A New Formulation of Anisotropic Equivalent Conductivity in Laminations," *IEEE Transactions on Magnetics,* vol. 47, no. 5, pp. 1378-1381, 2011.

[23] Ansys, Inc, "ANSYS Electromagnetics Suite 2020 R2 – Maxwell Help", Ansys, Inc, Canonsburg, PA, 2020

[24] T. Humiston and P. Pillay, "Parameter measurements to study surge propagation in induction machines," *IEEE Transactions on Industry Applications,* vol. 40, no. 5, pp. 1341-1348, 2004.

[25] X. Ju, Y. Cheng, M. Yang, S. Cui, A. Sun, X. Liu and M. He, "Voltage Stress Calculation and Measurement for Hairpin Winding of EV Traction Machines Driven by SiC MOSFET," *IEEE Transactions on Industrial Electronics,* vol. 69, no. 9, pp. 8803-8814, 2022.

[26] A. Hoffmann and B. Ponick, "Method to Predict the Non-Uniform Potential Distribution in Random Electrical Machine Windings under Pulse Voltage Stress," *Energies,* vol. 15, no. 358, 2022.

[27] Teledyne Lecroy, "Operator's Manual ADP300/305 Active Differential Probe Rev A," Teledyne Lecroy, New York, USA, 2013.

[28] A. Mbaye and T. Lebey, "Analytical approach of PD activity in low voltage motors fed by inverters [adjustable speed drives]," in *Proceedings of the 1998 IEEE 6th International Conference on Conduction and Breakdown in Solid Dielectrics*, 1998.

David A Hewitt received the MEng degree in Digital Electronics and PhD in Power Electronics from the University of Sheffield, UK in 2011 and 2016, respectively.

He is currently a Research Associate in Power Electronics with the Electrical Machines and Drives Group in the Department of Electronic and Electrical Engineering at the University of Sheffield, UK

His Research interests include reliability, condition monitoring and high frequency modelling of electric machines

Shubham Sundeep (Student Member, IEEE) received the B.Tech. degree in electrical engineering from the National Institute of Technology Surat, India in 2015, and the M.Tech. degree in power electronics, electrical machines, and drives from the Indian Institute of Technology, Delhi in 2017. He is currently pursuing the Ph.D. degree in electronics and electrical engineering with the Department of Electronics and Electrical Engineering, The University of Sheffield, Sheffield, U.K.

His research interests include condition monitoring, diagnostics, prognostics, and control of electrical machines, and electrical machine drives. Between 2017 and 2018, he was working as an R&D Engineer in EATON Corporation where he worked on the control of synchronous drives.

Jiabin Wang (Senior Member, IEEE) received the B.Eng. and M.Eng. degrees from Jiangsu University, Zhengjiang, China, in 1982 and 1986, respectively, and the Ph.D. degree from the University of East London, London, U.K., in 1996, all in electrical and electronic engineering. Currently, he is a Professor in Electrical Engineering at the University of Sheffield, Sheffield, U.K. From 1986 to 1991, he was with the Department of Electrical Engineering at Jiangsu University, where he was appointed a Lecturer in 1987 and an Associated Professor in 1990. He was a Postdoctoral Research Associate at the University of Sheffield, Sheffield, U.K., from 1996 to 1997, and a Senior Lecturer at the University of East London from 1998 to 2001. His research interests range from motion control and electromechanical energy conversion to electric drives for applications in automotive, renewable energy, household appliances, and aerospace sectors. He is a Fellow of the IET.

Antonio Griffo (Member, IEEE) received the M.Sc. degree in electronic engineering and the Ph.D. degree in electrical engineering from the University of Napoli "Federico II," Naples, Italy, in 2003 and 2007, respectively.

From 2007 to 2013, he was a Research Associate with the University of Sheffield, Sheffield, U.K., and the University of Bristol, Bristol, U.K. He is currently a Professor of Power Electronics and Electrical Drives with the Department of Electronic and Electrical Engineering, University of Sheffield. His research interests include modeling, control, and condition monitoring of electric power systems, power electronics converters, and electrical motor drives for renewable energy, automotive, and aerospace applications.